Electronic Supporting Information

for

Generating Plasmonic Heterostructures by Cation Exchange and Redox Reactions of Covellite CuS Nanocrystals with Au^{3+} Ions

Chao Hu[†a], Wenhui Chen[†a], Yi Xie[*a], Santosh Kumar Verma[a], Priscila Destro[b], Gang Zhan[a], Xingzhu Chen[a], Xiujian Zhao[a], P. James Schuck[c], Ilka Kriegel[*c,d], Liberato Manna[*d]

[a] State Key Laboratory of Silicate Materials for Architectures, Wuhan University of Technology (WUT), No. 122, Luoshi Road, Wuhan 430070, P. R. China

[b] Department of Chemical Engineering, Federal University of São Carlos (UFSCar), P.O. Box 676, 13565-905 São Carlos-SP, Brazil

[c] Molecular Foundry, Lawrence Berkeley National Laboratory, 1 Cyclotron Road, Berkeley, California 94720, United States

[d] Department of Nanochemistry, Istituto Italiano di Tecnologia (IIT), via Morego, 30, 16163 Genova, Italy

[†]These authors contributed equally to this work.

Email: xiey@whut.edu.cn

liberato.manna@iit.it

Ilka.Kriegel@iit.it

Contents

1. TEM images, XRD pattern and optical spectrum of the as-synthesized CuS NCs

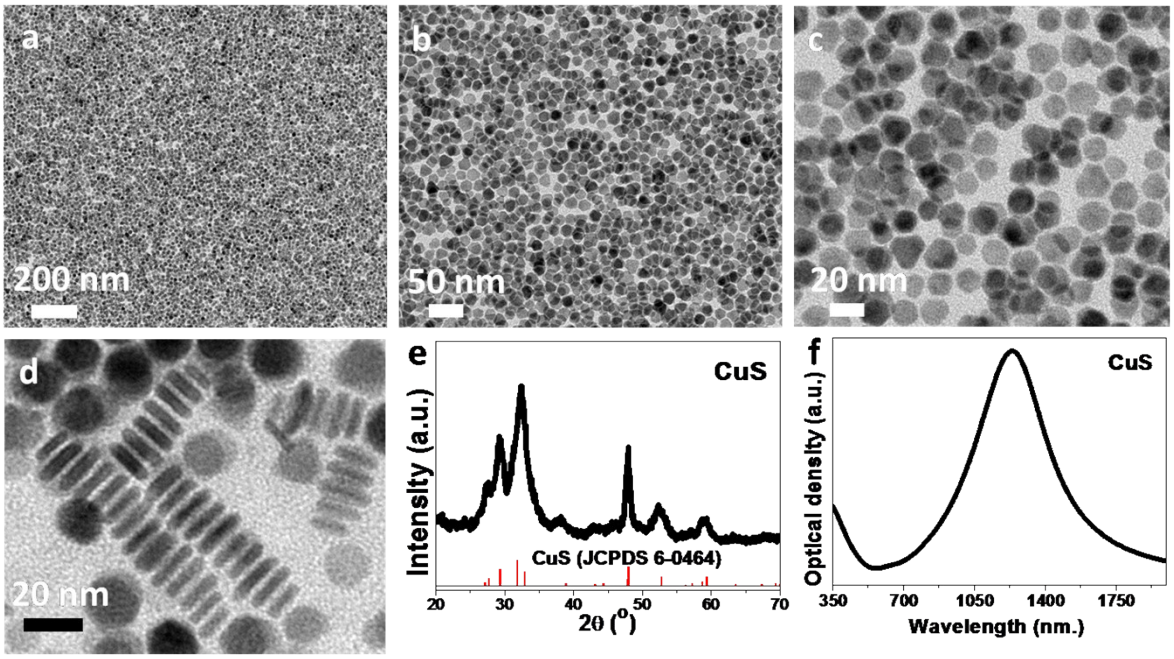

Fig. S1 (a-d) TEM images of covellite (CuS) nanocrystals (NCs) synthesized by using copper acetate monohydrate as precursor, at various magnifications showing the particle uniformity in size. (e-f) XRD pattern (e) and optical spectrum (f) of the corresponding NCs.

As shown in Fig. S1a-d, monodispersed nanoparticles (NPs) were achieved by heating up the mixture of copper acetate monohydrate ($C_4H_6CuO_4 \cdot H_2O$) and S pre-dissolved in oleylamine (OM) and octadecene (ODE) to 200 ^oC and keeping the reaction at this temperature for 30 min. The resulting nanoplates display average diameter and thickness of 18.6 ± 1.3 nm and 3.6 ± 0.5 nm, respectively. The aspect ratio (i.e. the diameter to thickness ratio) is higher than that of previously synthesized covellite (CuS) nanplates (with diameter and thickness of 13.0 ± 1.2 and 5.0 ± 0.4 nm, respectively) by using CuCl instead as Cu precursor.[1] The experimental XRD pattern of the collected nanocrystals (NCs) matches well with the covellite (CuS) phase (Fig. S1e, bottom). The as-synthesized CuS NCs exhibits well-defined NIR plasmon absorbance (Fig. S1f), which is slightly red-shifted compared with that of covellite (CuS) NCs previously reported by us.[1]

2. Characterization of the samples collected by reaction of CuS NCs with Au^{3+} in the absence of OM and AA

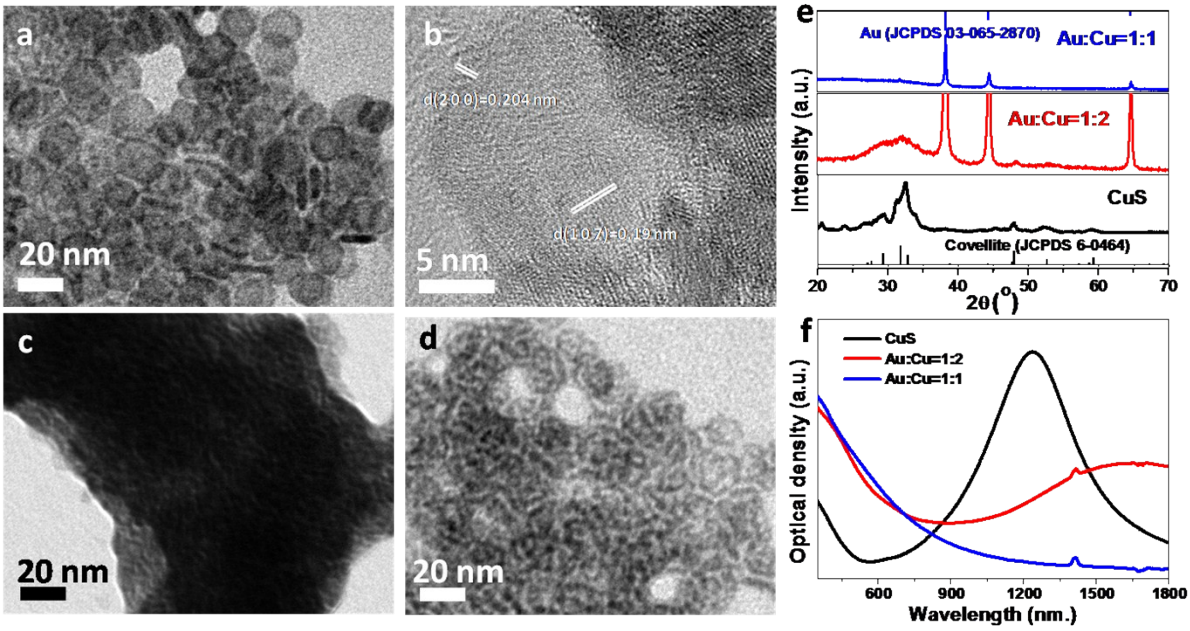

Fig. S2 (a-d) TEM images (a,c,d) and HRTEM (b) of NPs collected by reacting CuS with Au^{3+} alone (i.e. without OM and AA) by fixing precursor Au:Cu ratio as 1:2 (a-b) and 1:1 (c-d), respectively. (e-f) XRD patterns (e) and optical spectra (f) of the as-synthesized CuS and corresponding samples in panels a) and c), respectively.

Table S1. Summary of various representative reactions and related resulting nanostructures.

Reaction conditions	Nanostructures			Mechanism
	Au:Cu=1:2	Au:Cu=1:1	Au:Cu=2:1	
$CuS+Au^{3+}$	CuS@Au core-shell	Au NPs with hole		Redox reaction of CuS NPs with Au^{3+}
$CuS+AA+Au^{3+}$	CuS@Au core-shell	CuS@Au core-shell	Ring-like Au NPs	Redox reaction of Au^{3+} with CuS NPs and AA
$CuS+OM+Au^{3+}$	$CuS@Au_2S$	$CuS@Au_2S$	$CuS@Au_2S$	Cation exchange

	core-shell	core-shell	core-shell	
CuS+AA+OM+Au^{3+}	Au/CuS dimer	Au/CuS dimer	Au/CuS dimer	Redox reaction of Au^{3+} with AA

Table S2. Calculation of Cu and Au contents before and after reaction of the as-synthesized covellite (CuS) NCs with Au^{3+} alone (i.e. no AA, no OM). The calculation is based on ICP analysis.

	Before reaction		**After reaction**			
Samples	Cu in the starting NCs (μmol)	Initial Au amount (μmol)	Cu in the resulting NCs (μmol)	Cu left in the supernatant (μmol)	Au in the resulting NCs (μmol)	Au left in the supernatant (μmol)
CuS+Au^{3+}	12	6.0	3.99	7.01	4.98	0.39
CuS+Au^{3+}	12	12	2.20	10.18	9.74	2.06

Fig. S2 provides the TEM images, XRD patterns and optical spectra of the samples collected by reacting CuS NCs with Au^{3+} alone. The reaction led to heavy agglomeration of the NPs (Fig. S2a,c). The main experimental XRD peaks of the resulting NPs match well with metallic Au (Fig. S2e). Besides the strong diffraction peaks of metallic Au, relative weak peaks which could be indexed to covellite phase are preserved in the intermediated sample achieved with small amount of Au^{3+} ions (Fig. S2e, red curve). In this case, core-shell NPs were achieved (Fig. S2b). However, only diffraction peaks from metallic Au can be observed in the presence of more Au^{3+} ions (Fig. S2e, blue curve), and the initial CuS NPs were destroyed and cage-like NPs are formed (Fig. S2d). This might be due to the oxidation of CuS NPs by Au^{3+} ions. This redox reaction leads to the expelling Cu and S species from the parent CuS NPs to the solution, which is unambiguously evidenced from the ICP analysis on the resulting NPs and supernatant in a

representative reaction (Table S2). The rapid out-diffusion of Cu (S species as well) upon the redox reaction might explain the formation of holes in the NPs.

3. TEM images, XRD patterns and optical spectra of the samples collected by reaction of the CuS NCs with Au^{3+} in the presence of AA alone

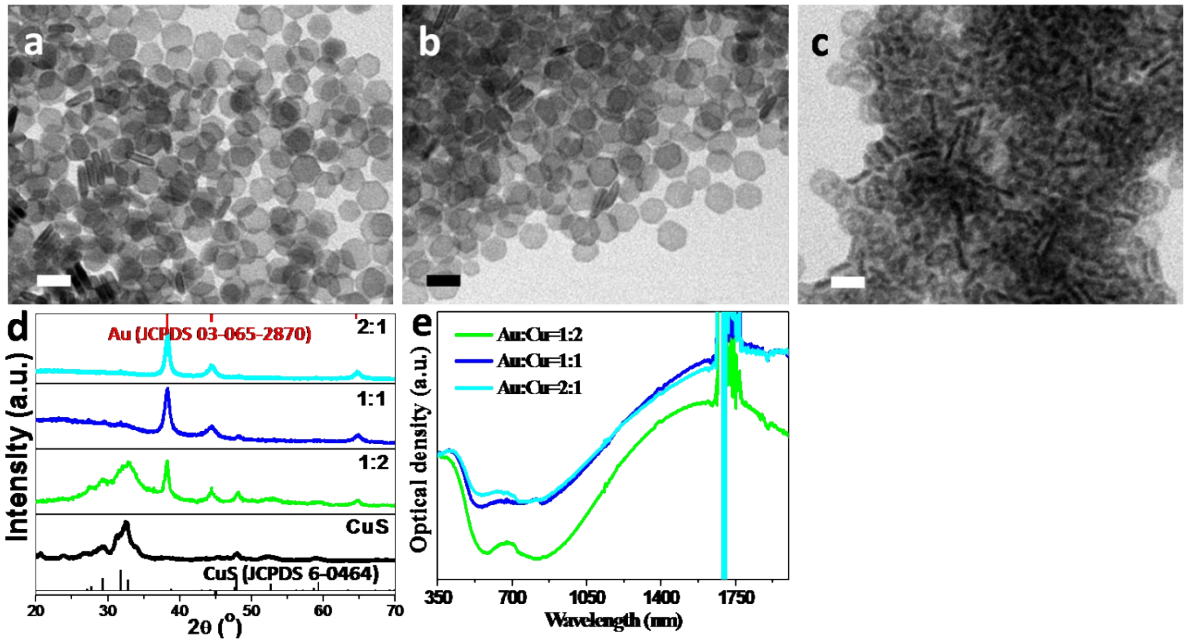

Fig. S3 (a-d) TEM images of the samples collected by the reaction of CuS with Au^{3+} in the presence of AA alone (i.e. without OM), with precursor Au:Cu ratios of 1:2 (a), 1:1 (b) and 2:1 (c). Each scale bar represents 20 nm. (d-e) XRD patterns (d) and optical spectra (e) of the corresponding sample achieved with different starting Au:Cu ratios as dictated.

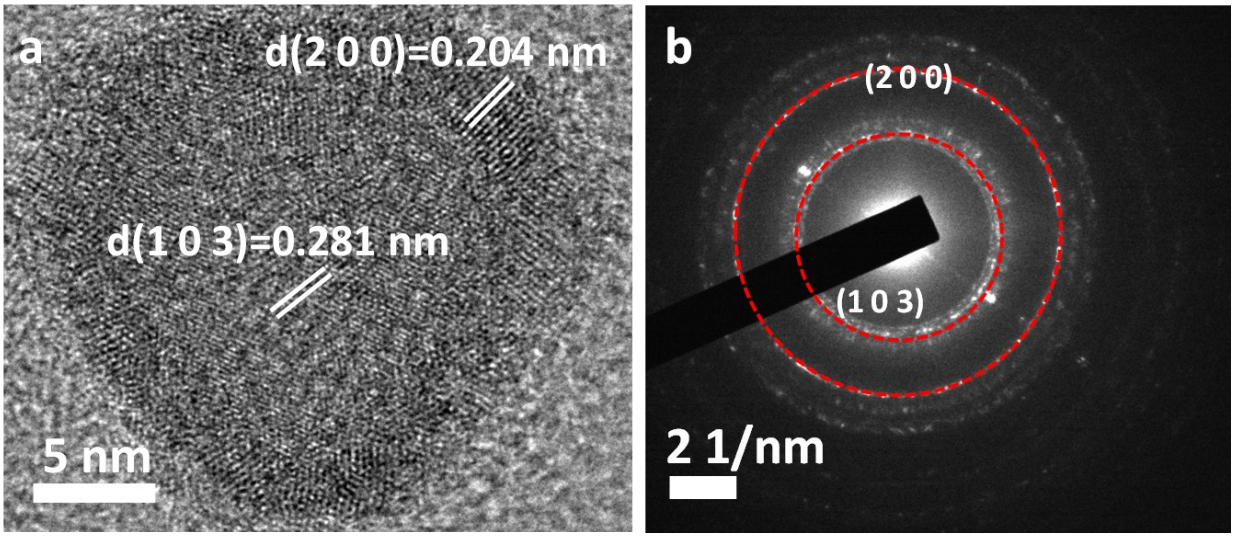

Fig. S4 HRTEM image (a) and SAED pattern (b) of the CuS@Au core-shell heterostructure achieved via reacting CuS with Au^{3+} ions in the presence of AA alone (i.e. without OM), by fixing precursor Au:Cu ratio as 1:1. The diffraction rings labeled (103) and (200) are attributed to diffraction from covellite CuS (JCPDS: 00-006-0464) and cubic Au (JCPDS: 03-065-2870), respectively.

We noticed that the control of the redox reaction between CuS NPs and Au^{3+} ions can be improved by the introduction of ascorbic acid (AA), a mild reducing agent. As reported in Fig. S3, core-shell nanostructures can be formed with small amount of Au^{3+} precursor, in the presence of AA. With increasing Au^{3+} amount the initial NPs are destroyed and ring-like NPs are generated (Fig. S3c-e). On the other side, the XRD patterns of the resulting NPs collected by reaction with less Au^{3+} ions (i.e. Au:Cu less than 2:1) evidence two sets of diffraction peaks, which are characteristic signals from covellite CuS (JCPDS No. 6-0464) and cubic Au phase (JCPDS No. 3-065-2870), respectively (Fig. S3f). The (111), (200) and (220) reflections originated from cubic Au at two theta of around 38.20°, 44.35° and 64.68° become sharper and more intense with increasing the precursor ratio of Au:Cu. The HRTEM analysis confirms the formation of cubic Au shell and the preserving covellite CuS core (Fig. S4a), and the selected area electron diffraction (SAED) pattern indicates the presence of both covellite CuS and cubic Au (Fig. S4b). We hypothesize that upon the oxidation, Au^{3+} ions adsorbed on the surface of NPs were reduced to $Au^{(0)}$. The Cu and S of the surface layer of CuS are expelled upon the redox

reaction, and thus metallic Au layer embedding CuS core is formed. With excess Au^{3+} ions the XRD patterns of the resulting NPs match with only cubic Au (Fig. S3f). These observations indicate that the ring-like NPs are most likely metallic Au.

4. Evolution of morphology, phase and optical spectra of various CuS@Au_2S core-shell NPs collected with varied precursor Au:Cu molar ratios in the presence of OM alone

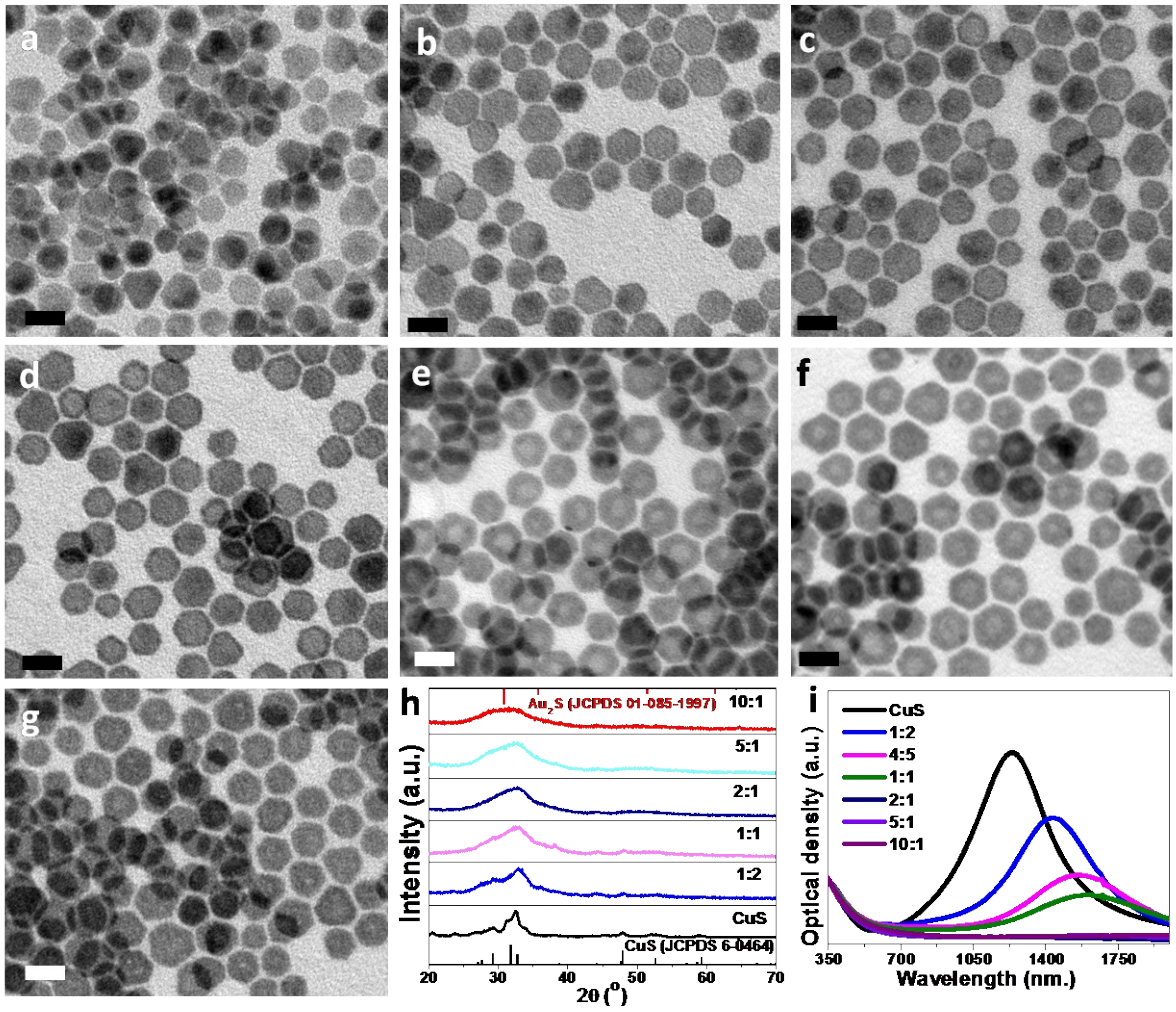

Fig. S5 (a-g) Evolution of morphologies from the as-synthesized CuS NCs (a) to CuS@Au_2S core-shell NPs with tunable shell thickness. The CuS@Au_2S samples are achieved by reacting CuS with Au^{3+} ion in the presence of OM alone (i.e. no AA), by fixing precursor Au:Cu molar ratios as 1:2 (b), 4:5 (c), 1:1 (d), 2:1 (e), 5:1 (f) and 10:1 (g). The scale bars are 20 nm. (h-i) Evolution of XRD patterns (h) and optical spectra (i) of the corresponding samples collected with different precursor Au:Cu molar ratios. The time for each reaction was 4 h.

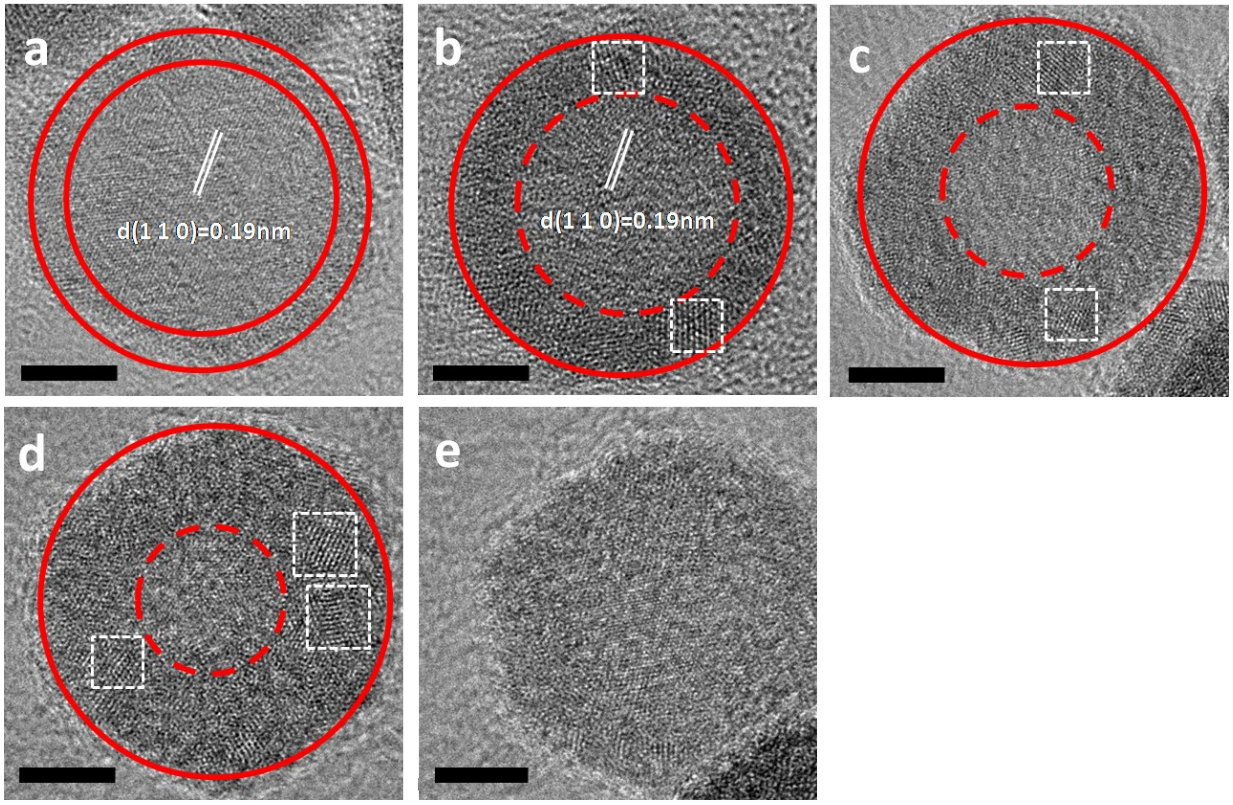

Fig. S6 HRTEM images (top view) of the representative CuS@Au_2S NPs collected with precursor Au:Cu molar ratios of 1:2 (a), 1:1 (b), 2:1 (c), 5:1 (d) and 10:1 (e), respectively. The scale bars are 5 nm.

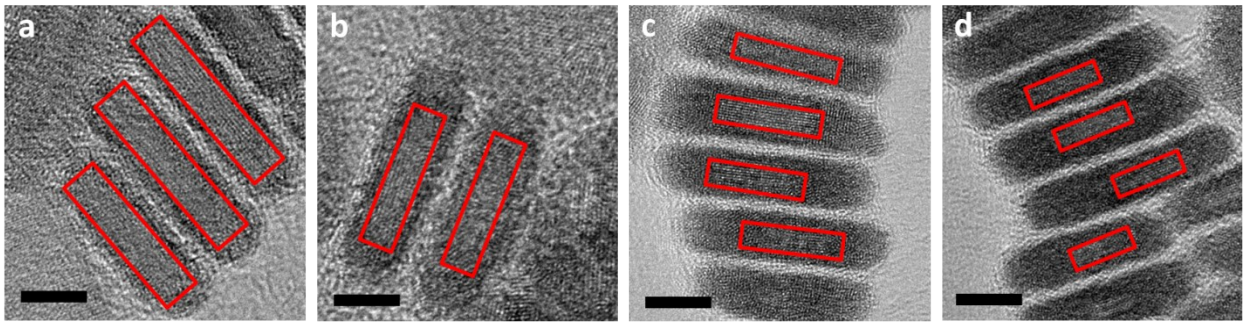

Fig. S7 HRTEM images (side view) of the representative CuS@Au_2S NPs collected with precursor Au:Cu molar ratios of 1:2 (a), 1:1 (b), 2:1 (c) and 5:1 (d), respectively. The scale bars are 5 nm.

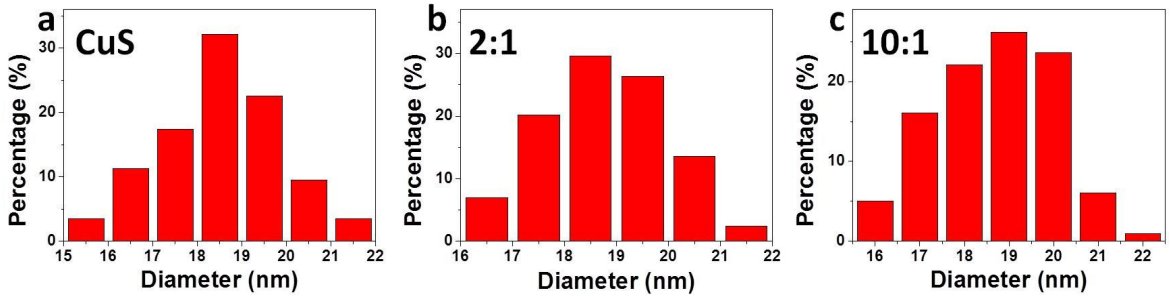

Fig. S8 Size distribution histogram (nanoplate diameter) of the as-synthesized CuS (a), and two representative CuS@Au_2S samples achieved by reacting CuS with Au^{3+} in the presence of OM alone (i.e. no AA), by fixing precursor Au:Cu as 2:1 (b) and 10:1 (c), respectively. The size is calculated from the representative TEM images shown in Fig. S5a, e, g, respectively. The average diameter of these samples from a-c are 18.6 ± 1.3 nm, 18.7 ± 1.2 nm and 18.8 ± 1.2 nm, respectively.

Table S3. Diameter and thickness of the core in the core-shell nanostructure achieved with different precursor Au:Cu molar ratios.

Precursor Au:Cu molar ratio	Core diameter (nm)	Core thickness (nm)	NIR plasmon peak (nm)
0:1 (CuS)	18.6	3.6	1239
1:2	15.0	2.6	1433
1:1	12.0	2.2	1604
2:1	9.2	1.7	-
5:1	5.9	1.3	-

Fig. S5 reports the evolution of morphology, phase and optical spectra of various NPs over the precursor Au:Cu ratios by reaction of the as-synthesized CuS with Au^{3+} ions at RT in the

presence of OM alone (i.e. without AA). It is noteworthy that the introduction of OM stabilizes the reaction and leads to the formation of core-shell heterostructures (Fig. S5b-g). The TEM images and size distribution histograms (Fig. S8) indicate that all the resulting NPs inherite the overall morphology and size of the plate-like CuS although the shell increases in size and concomitantly the core becomes smaller as the reaction proceeds (Table S3). Like in the formation of shell by reacting CuS with Pd^{2+} ions,[2] damping and red-shift of NIR plasmon absorption are observed with increasing shell thickness (Fig. 5i).

Unlike the cation exchange (CE) of $Cu_{2-x}S$ with Au^{3+} ions for fabrication of $Cu_{2-x}S@Au_2S$ core-shell structure at higher temperature of 55 ^oC, which leads to the formation of crystalline shell,[3] in our case the reaction of CuS with Au^{3+} ions at RT leads to instead the generation of amorphous-like shell. This can be clearly evidenced from the evolution of XRD patterns (Fig. S5h). The diffraction peaks matching with covellite phase are still visible in the samples achieved with low precursor Au:Cu ratios (e.g. no more than 1:1). However, these peaks vanished in the samples with more Au^{3+} ions, and the diffraction peaks at around 32.7^o broadened and evolved to one broad and weak diffraction peak centered at around 30^o with increasing Au^{3+} ions amount (Fig. S5h, red curve). This new emerging broad and weak peak could be attributed to the amorphous feature[2]. The spacing lattices of the core displayed in HRTEM images confirm the preservation of covellite phase (Fig. S6a-b). In addition, crystalline domains were observed in the shell according to HRTEM images, which would be discussed in detail in the next section.

5. Evolution of the morphology of the core-shell nanostructures upon E-beam irradiation

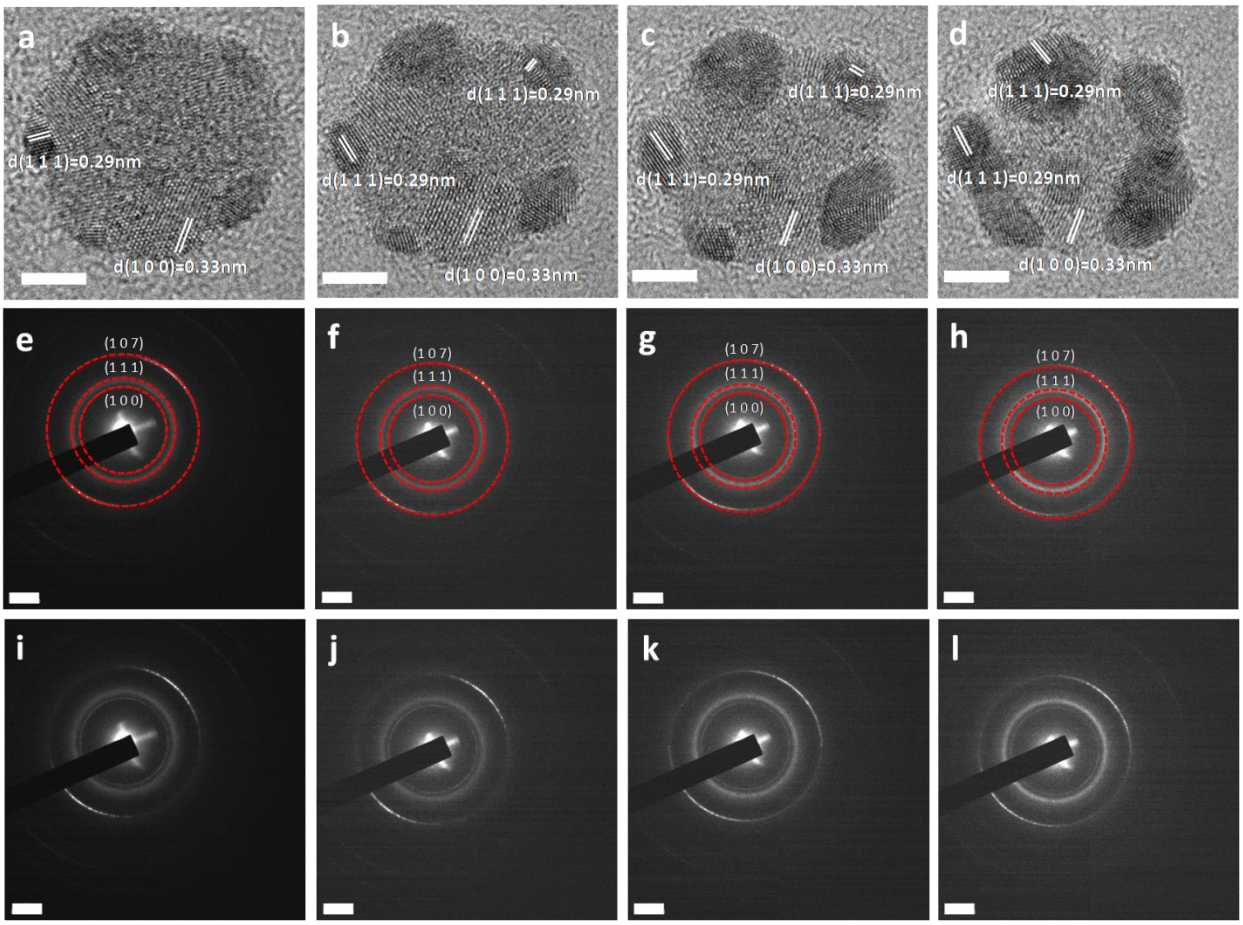

Fig. S9 (a-d) HRTEM observations on the single CuS@Au_2S core-shell NPs at different E-beam irradiation time during HRTEM measurement at a working voltage of 200 kV. From panel a) to panel d) the irradiation time increases. The scale bar of HRTEM images is 5 nm. (e-h) SAED patterns of the CuS@Au_2S samples collected at different E-beam irradiation time. The diffraction ring labeled (110) and (107) are attributed to diffraction from covellite CuS, and the (111) ring is attributed to cubic Au_2S (JCPDS No. 01-085-1997). (i-l) SAED patterns as shown in panels e-h), but without the marked red circles. The scale bar of SAED is 2 1/nm.

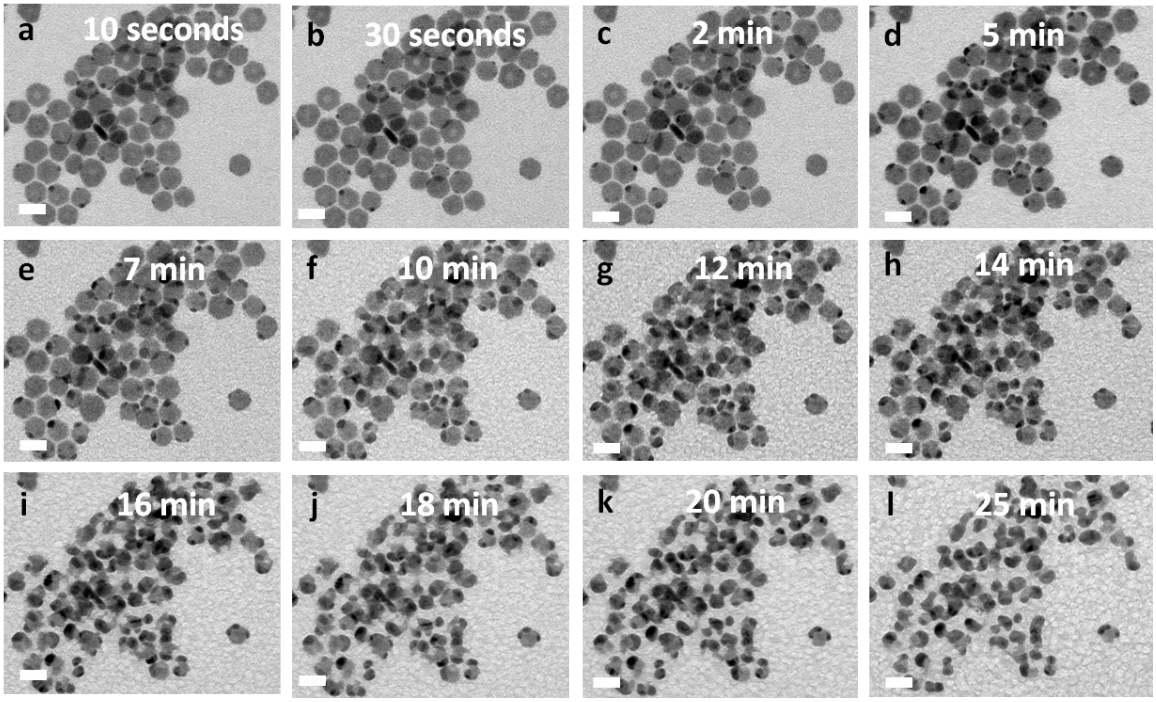

Fig. S10 Evolution of the TEM images of the CuS@Au_2S core-shell NPs observed at different E-beam irradiation time during TEM measurement at a working voltage of 100 kV. The scale bars are 20 nm.

As discussed above, crystalline feature is observed from HRTEM images. We noticed that the crystalline domains grow and become prominent as the E-beam irradiation proceeds, despite the working voltage at 200 kV or 100 kV (Figs. S9-10). This evolution is similar with the previously reported transformation from crystalline $Cu_{2-x}S$@Au_2S core-shell to segmented heterostructure,[3] except that in our case new emerged crystalline segments were due to the crystallization of the amorphous shell upon E-beam irradiation. Indeed, the lattice spacings of the planes in these new emerged domains of the shell are 0.29 nm, corresponding to the (111) planes of cubic Au_2S (Fig. S9a-d). The conversion from amorphous shell to crystalline domains is so rapid that it's difficult to collect HRTEM images of core-shell NPs displaying complete amorphous shell. Prolonging irradiation time leads to the destroying NPs (Fig. S10j-l).

6. Analysis of Cu and Au amount before and after the reaction of CuS with Au^{3+} in the presence of OM alone

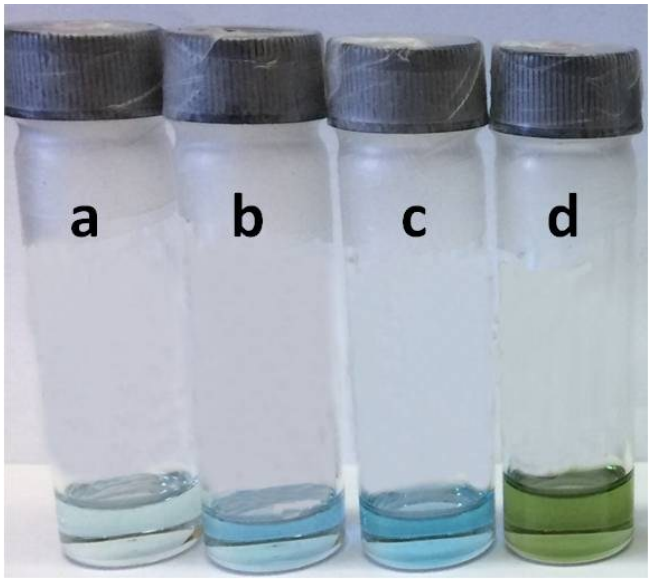

Fig. S11 Optical photos of the supernatants collected upon the reaction of CuS with Au^{3+} in the presence of OM alone (i.e. no AA), by fixing precursor Au:Cu ratios as 1:5 (a), 1:2 (b), 1:1 (c) and 2:1 (d), respectively. The color of the supernatant changed from light blue, blue, blue to green with increasing Au amount in the reaction.

Table S4. Calculation of Cu and Au amounts before and after reacting CuS NCs with different amounts of Au^{3+} in the presence of OM alone (i.e. no AA). The calculation is based on ICP tests and analyses.

	Before reaction		**After reaction**				
Samples	Cu in the parent CuS NCs (μmol)	Initial Au amount (μmol)	Cu left in the resulting NCs (μmol)	Cu released to the supernatant (μmol)	Au gained by the CuS NCs (μmol)	Au left in the supernatant (μmol)	[a]Molar ratio of $Cu_{released}$:Au_{gained}
Sample1	12	2.32	9.28	2.38	2.11	0.06	1.13:1

Sample2	12	4.64	6.47	4.77	3.84	0.54	1.24:1
Sample3	12	18.56	5.56	7.37	6.73	11.08	1.10:1
Sample4	12	120	2.14	11.81	11.40	101.32	1.04:1

[a] The $Cu_{released}$:Au_{gained} means the molar ratio of the Cu released from the starting CuS NCs to the solvent and the Au gained by the CuS NCs upon the reaction.

The reaction of CuS NCs with Au^{3+} ions in the presence of OM alone involves a cation exchange. The Cu^{+} ions release from CuS NCs to the solvent upon the substitution by Au^{3+} ions, and can be further oxidized to Cu^{2+} by Au^{3+} remaining in the solvent. Indeed, the blue and green colors of the supernatant after reaction indicate the presence of Cu^{2+} ions (Fig. S11). It is difficult to monitor the local elemental composition of the core and shell by using energy dispersive X-ray spectroscopy (EDS) elemental maps because the NPs are not stable under E-beam irradiation, as previously discussed. We thus employ the overall elemental analysis via ICP to compare the amount of Cu and Au before and after the reaction (Table S4). The Cu amount of the initial CuS NCs is 12 μmol for each reaction. As shown in Table S4, the sum of the Au gained by the CuS NCs and the Au left in the supernatant matches the initial Au amount added to the NC solution. In addition, the Au amount (μmol) gained by the starting CuS NCs equals around 1.10-1.24 instead of 3 times of the Cu amount (μmol) found in the solution. Based on the above calculation and analyses, we hypothesize the possible reaction mechanisms as follows:

a) Upon the cation exchange, two fractions of Au^{3+} ions (e.g. 2γ moles) from the solution phase (labeled as $2\gamma Au^{3+}$ (l)) enters the CuS NC lattice, which leads to the releasing 6γ moles Cu^{+} ions (labeled as $6\gamma Cu^{+}$ (l)) to the solution (Formula 1-1).
b) The released Cu^{+} ions (6γ moles) are oxidized to 6γ moles Cu^{2+} by Au^{3+} ions remaining in the solution, which concomitantly generated 3γ moles Au^{+} ions (Formula 1-2) or 2γ moles $Au^{(0)}$ (Formula 1-3).

c) The generated 3γ moles Au^{+} ions are further gained by CuS NCs via a cation exchange with the host Cu^{+} ions, but this time only equimolar amount of Cu^{+} (i.e. 3γ moles Cu^{+}) is repelled from CuS to the solvent (Formula 1-4).

d) The incorporation of the generated $Au^{(0)}$ species by the NPs can not be completely ruled out. Once the $Au^{(0)}$ diffuse into the NPs, it might provide electrons to the covalent S-S bonds, which leads to the formation of Au^{+} and S^{2-}. Concomitantly Cu^{+} ions are kicked out (Formula 1-5).

e) Overall the reaction can be summarized as Formula (1-6). Based on formula (1-6) the inflowing 5γ moles Au^{3+} ions from the solution to the NC lattice leads to the formation of 6γ moles Cu^{2+} and 3γ moles Cu^{+} in the solution. That is, 9γ moles of Cu^{+} is released from the starting CuS NPs. Keep in mind that even the 3γ moles Cu^{+} can further react with Au^{3+} left in the solution like the reaction shown in Formulae (1-2) and (1-3), the final exchange ratio of Cu:Au is much less than 3:1. This explains the experimental ICP analyses reported in Table S4.

$$CuS\ (s) + 2\gamma Au^{3+}\ (l) \rightarrow Au_{2\gamma}S_{\gamma}\ (shell) + Cu_{1-6\gamma}S_{1-6\gamma}\ (core) + 6\gamma Cu^{+}\ (l) + 5\gamma S\ (l) \qquad (1\text{-}1)$$

$$6\gamma Cu^{+}\ (l) + 3\gamma Au^{3+}\ (l) \rightarrow 6\gamma Cu^{2+}\ (l) + 3\gamma Au^{+}\ (l) \qquad (1\text{-}2)$$

$$6\gamma Cu^{+}\ (l) + 2\gamma Au^{3+}\ (l) \rightarrow 6\gamma Cu^{2+}\ (l) + 2\gamma Au^{(0)}\ (l) \qquad (1\text{-}3)$$

$$CuS\ (s) + 3\gamma Au^{+}\ (l) \rightarrow 3/2Au_{2\gamma}S_{\gamma}\ (shell) + Cu_{1-3\gamma}S_{1-3\gamma}\ (core) + 3\gamma Cu^{+}\ (l) + 3/2\gamma S\ (l) \qquad (1\text{-}4)$$

$$CuS\ (s) + 3\gamma Au^{(0)}\ (l) \rightarrow 3/2Au_{2\gamma}S_{\gamma}\ (shell) + Cu_{1-3\gamma}S_{1-3\gamma}\ (core) + 3\gamma Cu^{+}\ (l) + 3/2\gamma S\ (l) \qquad (1\text{-}5)$$

Formula (1-1), (1-2) and (1-4) could be further summarized as follows:

$$2CuS\ (s) + 5\gamma Au^{3+}\ (l) \rightarrow 5/2Au_{2\gamma}S_{\gamma}\ (shell) + Cu_{2-9\gamma}S_{2-9\gamma}\ (core) + 6\gamma Cu^{2+}\ (l) + 3\gamma Cu^{+}\ (l) + 13/2\gamma S\ (l) \qquad (1\text{-}6)$$

All these results verified that the RT reaction of CuS with Au^{3+} in the presence of OM alone involves mainly a cation exchange process, which allows us a CuS@Au_2S core-shell heterostructure.

7. Characterization of the core-shell heterostructure collected at different time by reacting CuS NCs with Au^{3+} ions in the presence of OM alone

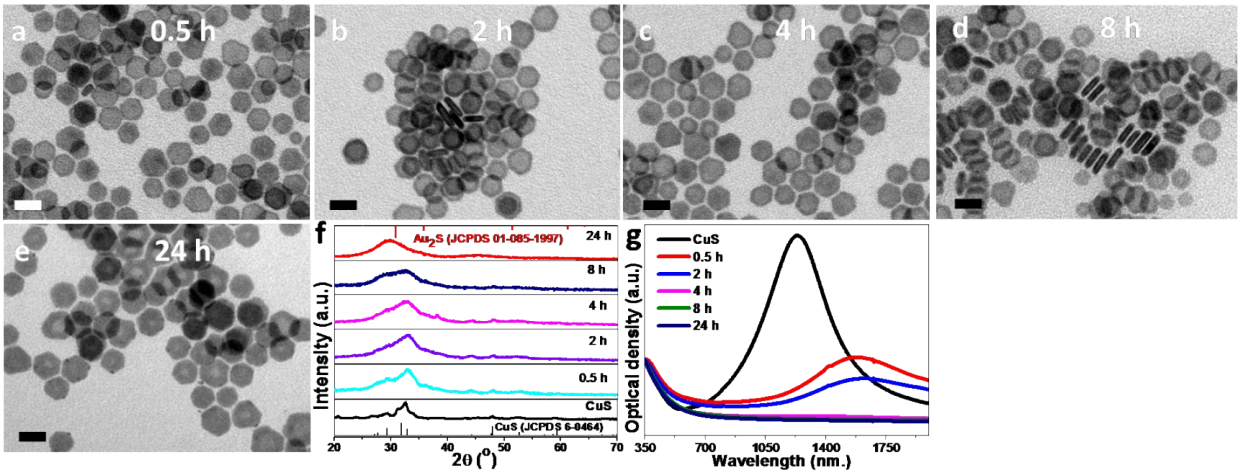

Fig. S12 (a-e) TEM images of the as-synthesized CuS and the NPs collected at different time by reacting CuS NCs with Au^{3+}cations in the presence of OM alone. The scale bar is 20 nm. (f-g) XRD patterns (f) and optical spectra (g) of the corresponding samples. The starting Au:Cu molar ratio is 2:1.

The overall morphology and size of the NPs can be preserved, however the shell increased in size with prolonging reaction time (Fig. S12a-e). The XRD peaks at two theta of 29.3° and 32.7° progressively evolve to one broad and weak peak as the reaction proceeds within 24 h, which confirms the amorphorization of the initial covellite NCs.

8. Characterization of the samples collected at different reaction temperatures in the presence of OM alone

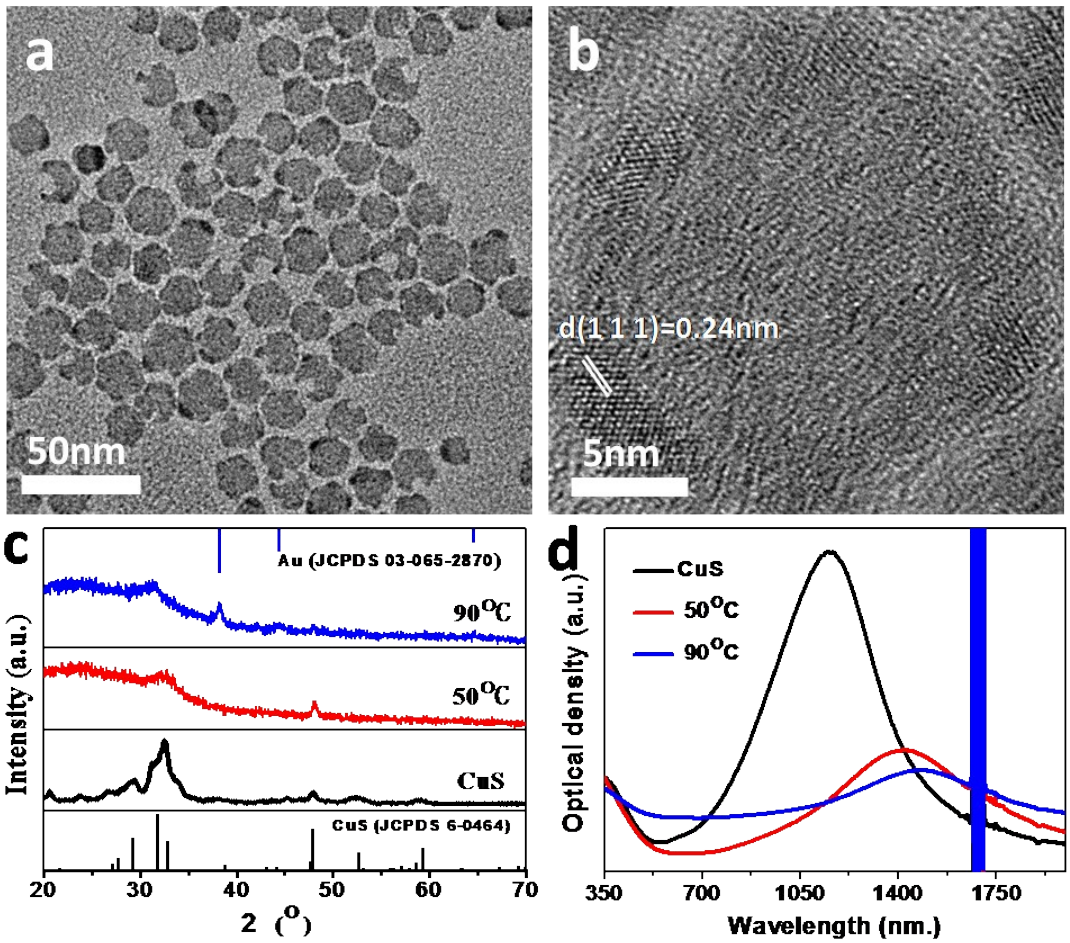

Fig. S13 (a-b) TEM (a) and HRTEM (b) images of the samples achieved at 90 °C in the presence of OM alone. (c-d) XRD patterns (c) and optical spectra (d) of the samples collected at 50 °C and 90 °C, respectively.

For comparison, we also tried the reaction at higher temperature of 50 °C and 90 °C, respectively. Unlike the previously reported reaction of $Cu_{2-x}S$ with Au^{3+} ions at 55 °C, which generated crystalline $Cu_{2-x}S@Au_2S$ core-shell nanostructure,[3] in our case the reacting covellite with Au^{3+} at 90 °C yield instead the etched NPs with segmented heterostructure (Fig. S13a-b). We noted that in this case neither amorphous feature nor crystalline Au_2S could be evidenced from XRD analysis. Instead, besides initial peaks attributed to covellite phase, the new emerged

diffraction peaks can be indexed to metallic Au phase (Fig. S13c, blue curve). Indeed, the lattice analysis based on HRTEM confirms the formation of Au domains in the segmented NPs (Fig. S13b). Consequently, the reaction of CuS NCs with Au^{3+} ions at high temperature involved more likely a redox process, in which Au^{3+} was reduced to metallic Au domain.

9. TEM images, XRD patterns and optical spectra of Au/CuS dimers obtained by reaction of CuS with different amounts of Au^{3+} ions in the presence of both OM and AA

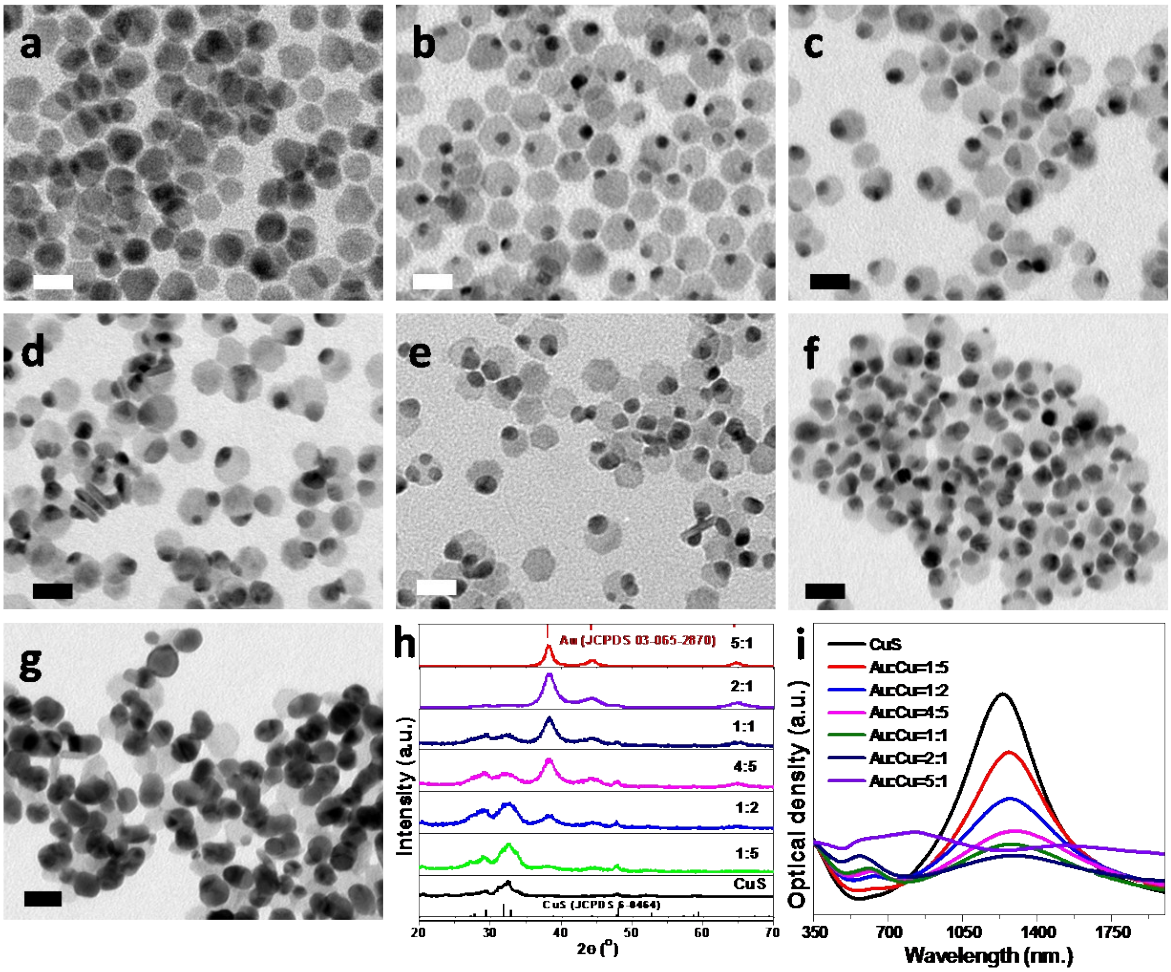

Fig. S14 (a-g) TEM images of the as-synthesized CuS NCs (a) and Au-CuS dimers achieved with precursor Au:Cu molar ratios of 1:5 (b), 1:2 (c), 4:5 (d), 1:1 (e), 2:1 (f) and 5:1 (g). The scale bar is 20 nm. (h-i) XRD patterns (h) and optical spectra (i) of the corresponding samples shown in panels a-g).

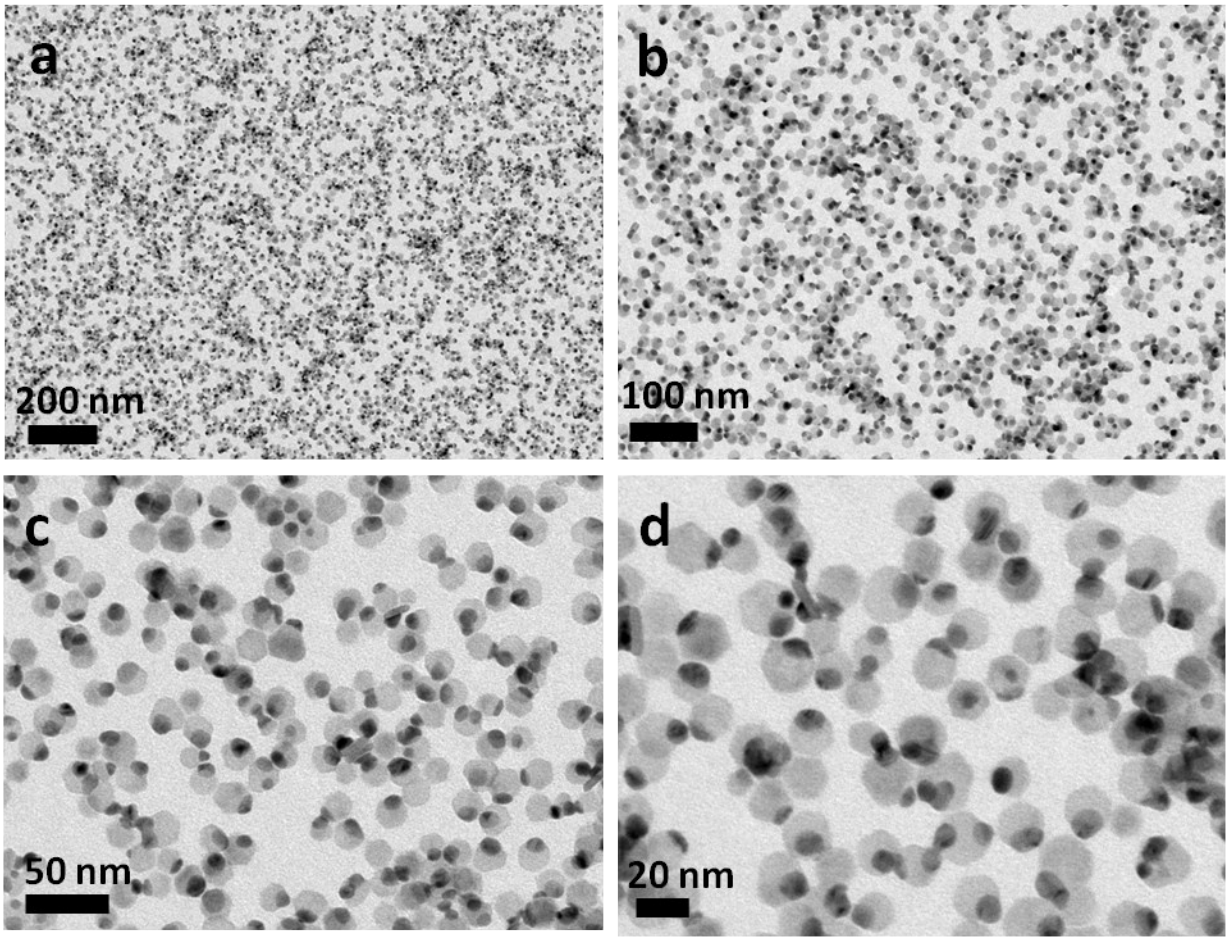

Fig. S15 TEM images of Au/CuS dimers with different magnifications. The precursor Au:Cu ratio is 1:1.

Table S5. Summary of the parameters of the CuS/Au dimers: size dimensions of Au domains (average diameter) and experimental plasmon peak position (λ_{exp}) in visible and NIR regions, respectively. The dimensions are calculated based on TEM analyses. The size of the CuS substrate is the same as the parent CuS (i.e. d×h=18.6×3.6 nm).

Au:Cu	Diameter of Au (found by TEM analysis) (nm)	λ_{exp} of CuS domain (nm)	λ_{exp} of Au domain (nm)
0:1 (**CuS** NPs)	-	1239	-

1:2	8.0	1274	637
1:1	9.1	1278	611
2:1	11.1	1291	566

It is interesting that the introduction of both OM and AA leads to the generation of dimers instead of core-shell nanostructure. The dimers are composed of initial CuS and metallic Au domains, as convinced by the evolution of TEM/HRTEM images and XRD patterns (Fig. S14a-h and Fig. 3 of the main text). Overall, the experimental XRD patterns indicate the presence of both covellite (CuS) phase (JCPDS No. 00-006-0464) and cubic Au phase (JCPDS No. 03-065-2870) in the resulting dimers. The diffraction peaks of cubic Au become sharper and more intense with increasing the starting Au:Cu ratio from 1:5 to 5:1, and in the meantime the peaks originated from covellite decrease in intensity. The covellite CuS domains of the dimers preserve their shape and size, however the Au segments become larger with the increasing Au^{3+} amount in the reaction (Fig. S14b-g).

It is noteworthy that the resulting Au/CuS dimers show two sets of absorbance bands in the visible and NIR regions, which are assigned to the localized surface plasmon resonances (LSPRs) of Au and CuS domains, respectively (Fig. S14i). The visible plasmon absorbance of Au increases in intensity with increasing Au^{3+} ions added, and concomitantly the intensity of the NIR plasmon absorbance from CuS decreases relatively. These results allow us the fabrication of metal/semiconductor dimers with dual plasmon bands in both visible and NIR regions.

10. TEM images, XRD patterns and optical spectra of the Au/CuS dimers achieved at different reaction time in the presence of both AA and OM

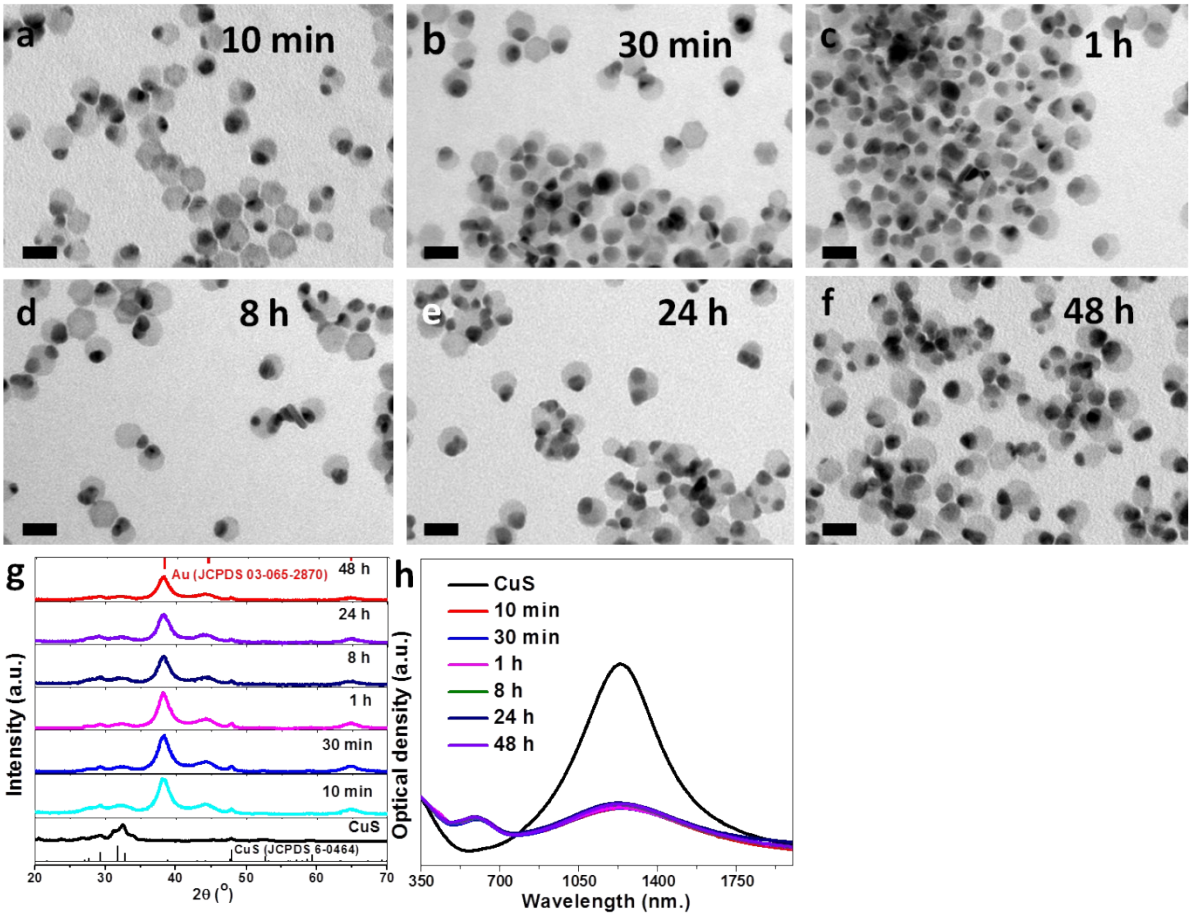

Fig. S16 (a-f) TEM images of Au/CuS dimers collected at different reaction time as dictated. (g-h) XRD patterns (g) and optical spectra (h) of the corresponding samples. Precursor Au:Cu ratio is 2:1. The scale bar is 20 nm.

11. Influence of AA amount on the TEM images, XRD patterns and optical spectra of Au/CuS dimers

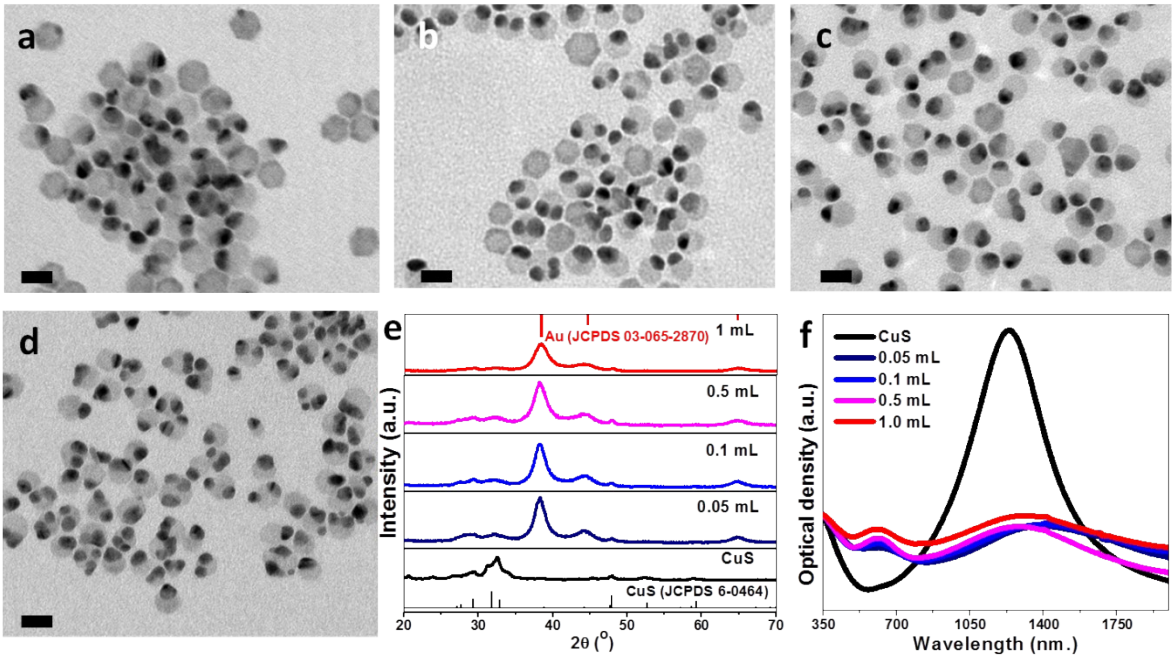

Fig. S17 (a-d) TEM images of Au/CuS dimers achieved with varied AA amounts of 0.05 mL (a), 0.1 mL (b), 0.5 mL (c) and 1.0 mL (d), respectively. The scale bar is 20 nm. (e-f) XRD patterns (e) and optical spectra (f) of the corresponding samples. For reference, the XRD pattern and optical spectrum of CuS are also provided in panels e) and f), respectively.

12. Theoretical framework and simulation of plasmon absorbance

$$\varepsilon_{Drude} = \varepsilon_{\infty} - \frac{\omega_p^2}{(\omega^2 + i\omega\gamma)}$$

Where ε_{Drude} is the dielectric function based on the Drude model with ω_p being the plasma frequency of the material, ε_∞ is the high frequency dielectric constant, and γ is the carrier damping. For CuS we chose the values as extracted from previously-reported work,[4] while for gold the bulk dielectric function was used.[5]

The ellipsoid was simulated using the following formulation:

Volume particle

$$V = 4/3 \cdot \pi \cdot \left(\frac{d_{core-shell}}{2}\right)^2 \cdot \left(\frac{h_{core-shell}}{2}\right)$$

aspect ratio: diameter/height

$$r = d/h$$

$$e = \sqrt{1 - \frac{1}{r^2}}$$

$$g = \sqrt{\frac{(1 - e^2)}{e^2}}$$

Depolarization factors for oblate with $L_a < L_b = L_c$

$$L_b = \left(\frac{g}{2e^2}\right) \cdot \left(\frac{\pi}{2} - \tan^{-1} g\right) - \frac{g^2}{2}$$

$$L_a = \frac{(1 - L_b)}{2}$$

Polarizability

$$\alpha = \varepsilon_0 \cdot V \cdot \frac{1}{3}\left(\frac{\varepsilon_p - \varepsilon_H}{3L_a(\varepsilon_p - \varepsilon_H) + 3\varepsilon_H}\right) + \frac{2}{3}\left(\frac{\varepsilon_p - \varepsilon_H}{3L_b(\varepsilon_p - \varepsilon_H) + 3\varepsilon_H}\right)$$

Polarizability for core-shell ellipsoid:

$$\alpha = \varepsilon_0 \cdot V \cdot \frac{1}{3}\left(\frac{(\varepsilon_p - \varepsilon_H)}{3 \cdot L_a(\varepsilon_p - \varepsilon_H) + 3 \cdot \varepsilon_H}\right) + \frac{2}{3}\left(\frac{(\varepsilon_p - \varepsilon_H)}{3 \cdot L_b(\varepsilon_p - \varepsilon_H) + 3 \cdot \varepsilon_H}\right)$$

$$C_{ext} = 2\pi \cdot \lambda \cdot \sqrt{\varepsilon_H} \cdot Im(\alpha)$$

Instead the core-shell ellipsoids were calculated based on an effective medium approximation,[6] and briefly outlined below:

Depolarization factors for material 1 and 2 (core and shell, respectively) for the special case of the semi-axis a and b=c.

$$N_{a1} = \frac{1}{(1 + 1.6 \cdot \frac{a_1}{b_1} + 0.4 \cdot \left(\frac{a_1}{a_1}\right)^2)}$$

$$N_{b1} = 0.5 \cdot (1 - N_{a1})$$

$$N_{a2} = \frac{1}{(1 + 1.6 \cdot \frac{a_1}{b_1} + 0.4 \cdot \left(\frac{a_2}{a_2}\right)^2)}$$

$$N_{b2} = 0.5 \cdot (1 - N_{a2})$$

Thus the volume of the ellipsoid gets:

$$V_1 = 4/3 \cdot \pi \cdot (a_1 \cdot b_1^2)$$

$$V_2 = 4/3 \cdot \pi \cdot (a_2 \cdot b_2^2)$$

Volume fraction for ellipsoids:

$$f_{V1} = \frac{V_1}{V_{total}}$$

$$f_{V2} = \frac{V_2}{V_{total}}$$

Polarizability in a direction:

$$\alpha_a = (f_{V1} + f_{V2}) \cdot \left\{ \left[(\varepsilon_1 - \varepsilon_0) + \left[\varepsilon_1 + N_{a1} \cdot (\varepsilon_0 - \varepsilon_1) \right] \cdot \frac{(\varepsilon_2 - \varepsilon_1) \cdot \frac{V_2}{V_1 + V_2}}{(\varepsilon_1 + N_{a2} \cdot (\varepsilon_2 - \varepsilon_1)} \right] \cdot \left[[\varepsilon_0 + N_{a1} \cdot (\right.$$

$$\alpha_{ab} = (f_{V1} + f_{V2}) \cdot \left\{ \left[(\varepsilon_1 - \varepsilon_0) + \left[\varepsilon_1 + N_{b1} \cdot (\varepsilon_0 - \varepsilon_1) \right] \cdot \frac{(\varepsilon_2 - \varepsilon_1) \cdot \frac{V_2}{V_1 + V_2}}{(\varepsilon_1 + N_{b2} \cdot (\varepsilon_2 - \varepsilon_1)} \right] \cdot \left[[\varepsilon_0 + N_{b1} \cdot \right.$$

The effective dielectric function is then calculated as:

$$\varepsilon_{eff} = \varepsilon_0 \cdot \frac{(\alpha_a + 2\alpha_b)}{(1 - N_{a1} \cdot \alpha_a - 2 \cdot N_{b1} \cdot \alpha_b)}$$

And the absorbance is then calculated as:

$$A = Im(\sqrt{\varepsilon_{eff}})$$

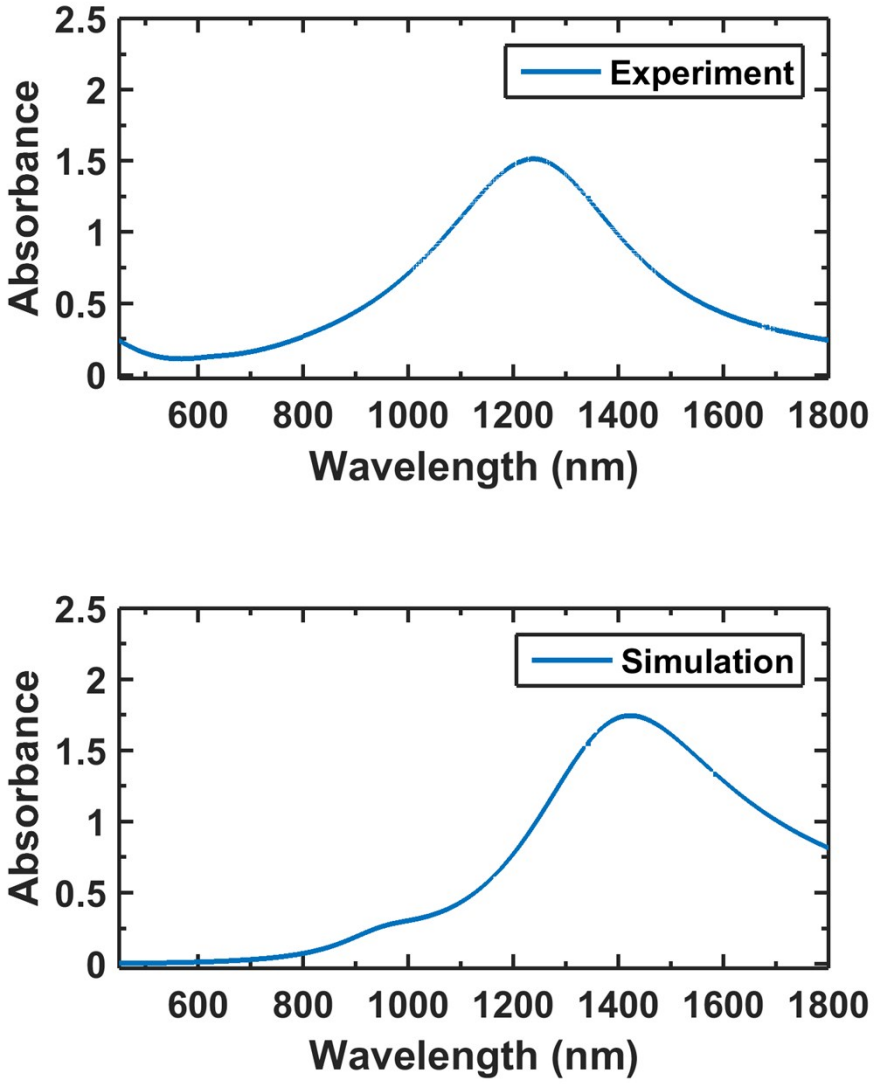

Fig. S18 Comparison of experimental and theoretically-simulated optical spectra of synthesized CuS NCs of 3.6×18.6 nm (height × diameter) dimensions.

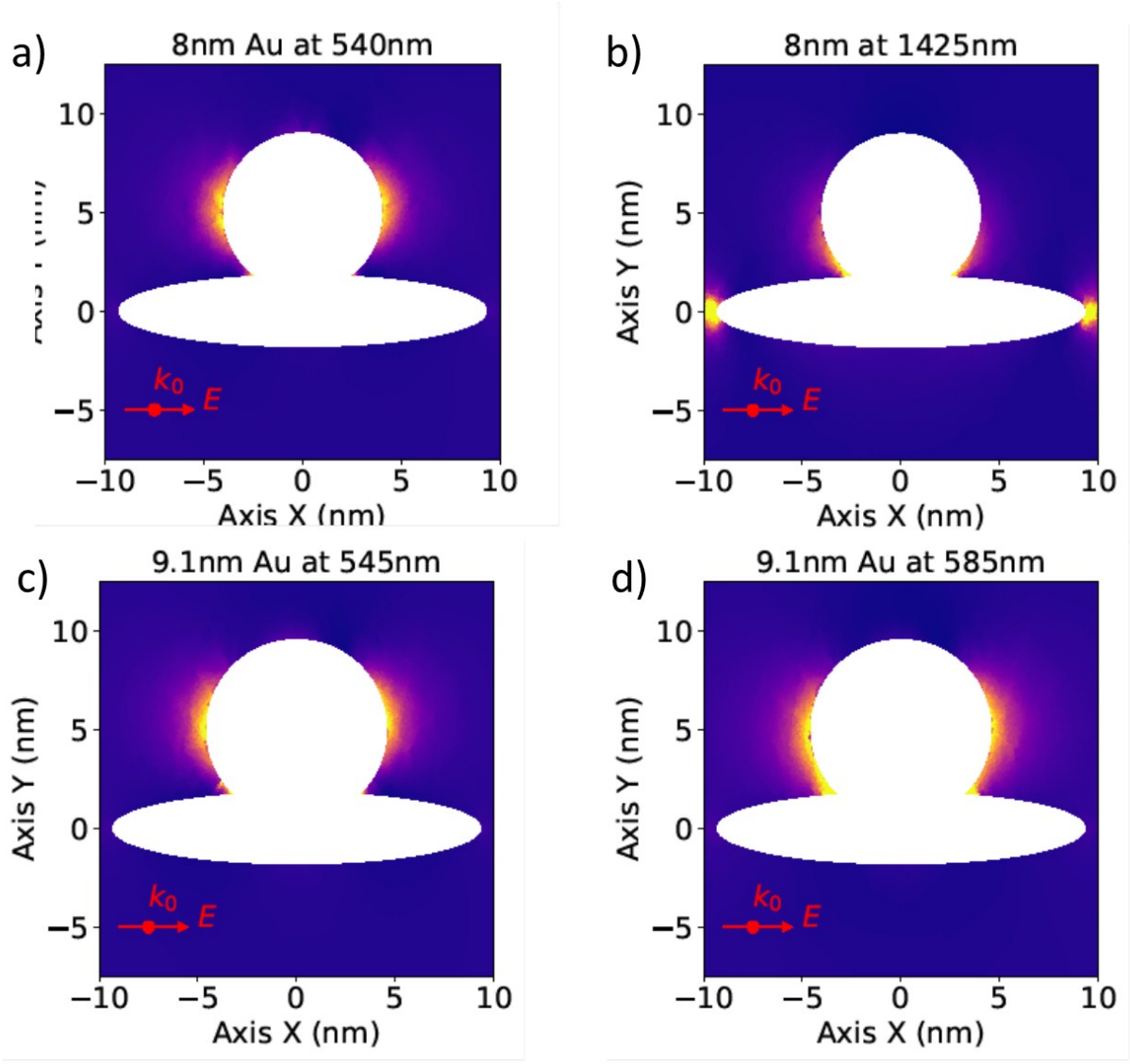

Fig. S19 Illustration of the near field enhancement surrounding the NP after excitation along and across the main axis of the NP.

References

1. Y. Xie, A. Riedinger, M. Prato, A. Casu, A. Genovese, P. Guardia, S. Sottini, C. Sangregorio, K. Miszta, S. Ghosh, T. Pellegrino and L. Manna, *J. Am. Chem. Soc.*, 2013, **135**, 17630-17637.
2. Y. Xie, W. Chen, G. Bertoni, I. Kriegel, M. Xiong, N. Li, M. Prato, A. Riedinger, A. Sathya and L. Manna, *Chem. Mater.*, 2017, **29**, 1716-1723.
3. X. Wang, X. Liu, D. Zhu and M. T. Swihart, *Nanoscale*, 2014, **6**, 8852-8857.
4. Y. Xie, L. Carbone, C. Nobile, V. Grillo, S. D'Agostino, F. Della Sala, C. Giannini, D. Altamura, C. Oelsner, C. Kryschi and P. D. Cozzoli, *ACS Nano*, 2013, **7**, 7352-7369.
5. P. B. Johnson and R. W. Christy, *Phys. Rev. B*, 1972, **6**, 4370-4379.
6. S. B. Jones and S. P. Friedman, *Water Resour. Res.* , 2000, **36**, 2821-2833.